Available online at www.sciencedirect.com
ScienceDirect
Polymer Degradation and Stability 93 (2008) 627–639
Polymer Degradation and Stability
www.elsevier.com/locate/polydegstab

Study on thermal degradation and combustion behaviors of PC/POSS hybrids

Lei Song*, Qingliang He, Yuan Hu, Hao Chen, Lei Liu

State Key Lab of Fire Science, University of Science and Technology of China, Hefei, Anhui 230026, PR China

Received 21 November 2007; received in revised form 24 December 2007; accepted 9 January 2008
Available online 25 January 2008

Abstract

Polycarbonate/polyhedral oligomeric silsesquioxane hybrids were prepared based on bisphenol A polycarbonate (PC) and trisilanolphenyl-POSS (TPOSS) by the melt blending method. Investigation of transmission electronic microscopy and Fourier transform infrared spectroscopy confirms that the nanoscale TPOSS particles were well dispersed in the PC matrix and there is no chemical reaction between the TPOSS particles and PC matrix during the melt blending. The thermal degradation behaviors of the PC/TPOSS hybrids were investigated. The presence of TPOSS significantly affects the thermal degradation process of PC. The combustion behaviors of the hybrids were evaluated by cone calorimetry experiments. The addition of TPOSS significantly decreased the value of peak heat release rate of the hybrids. Moreover, the addition of TPOSS at 2 wt% leads to the maximum decrease of the PHRR. And scanning electron microscopy and X-ray photoelectron spectroscopy were used to explore the char residues of the pure PC and the hybrids.

Keywords: Polycarbonate; Polyhedral oligomeric silsesquioxane; Melt blending; Thermal stability; Combustion behavior

1. Introduction

In recent years, polyhedral oligomeric silsesquioxanes (POSS) have attracted much interest of the academic and industrial researchers. POSS have a cage-like structure with 1–3 nm particle size. Their chemical composition can be represented as $(RSiO_{1.5})_n$ which is intermediate between silica and silicones $(R_2SiO)_x$, where R can be hydrogen or any alkyl, alkylene, aryl, arylene groups, or organo-functional derivatives thereof [1–4]. A large number of POSS derivatives have been synthesized that possess a similar characteristic structure containing a stable inorganic Si–O cage surrounded by organic substituents which can be modified to present a wide range of polarities and reactivities [5–23]. Polymer/POSS hybrids can be prepared through melt blending, grafting or copolymerization [5–23]. The incorporation of POSS which is regarded as a nanoscale filler is expected to lead to new or enhanced properties [5–23]. The preparations, morphology, crystallization, rheological behaviors, mechanical, thermal and flame retardant properties of the hybrids were reported. Zhao and Schiraldi [23] studied the mechanical properties of PC/POSS derivatives' composites. They found that the mechanical properties including tensile and dynamic mechanical moduli were slightly enhanced with the increase of trisilanolphenyl-POSS loading.

Bisphenol A polycarbonate (PC) is one of the most widely used engineering thermoplastics in the family of polycarbonate due to excellent properties, such as transparency, high mechanical strength, good thermal stability and flame retardancy. PC is an amorphous polymer with a relatively high glass transition temperature, $T_g = 140–150$ °C [24]. PC shows a V-2 rating in the UL-94 test because PC is a naturally high charring polymer, but strict flame retardant performance is often required. Many academic and industrial researchers have participated in the study of flame retardancy of PC and its blends [25]. The effective halogen-free flame retardants for PC include some phosphorus-, sulfur- and silicone-based flame retardants [25].

* Corresponding author. Tel./fax: +86 551 3601664.
E-mail address: leisong@ustc.edu.cn (L. Song).

0141-3910/$ - see front matter © 2008 Elsevier Ltd. All rights reserved.
doi:10.1016/j.polymdegradstab.2008.01.014

The major volatile degradation products are carbon dioxide, bisphenol A, carbon monoxide, methane, phenol, diphenyl carbonate, and 2-(4-hydroxyphenyl)-2-phenylpropane [26]. The minor products are ethylphenol, isopropenylphenol, isopropylphenol, and cresol [27]. Lee [27] and Jang and Wilke [28] studied the thermal degradation of PC in air. They found that the thermal oxidative degradation process of PC includes chain scission of the isopropylidene linkage and hydrolysis/alcoholysis of carbonate linkage. Oxygen may promote the branching and crosslinking as well as radical formation via the formation of peroxides in the beginning stage of degradation. These peroxides undergo further dissociations and combinations, producing aldehydes, ketones and some branched and crosslinked structures with diaryl ester, ether and unsaturated carbonaceous bridges at the surface of degraded polymer.

The current work reports the preparation of PC/POSS hybrids with different contents of POSS and the thermal degradation and the combustion behaviors of PC/POSS. The thermal degradation mechanism of PC/TPOSS hybrid is investigated and discussed.

2. Experimental

2.1. Materials

Bisphenol A polycarbonate (PC) (Scheme 1) was purchased from Dow Chemical Company. Trisilanolphenyl-POSS ($C_{42}H_{38}O_{12}Si_7$, molecular weight = 931.34 g/mol) was purchased from Hybrid Plastics Company. Prior to melt blending the PC pellets were dried for about 24 h under vacuum at 100 °C. Trisilanolphenyl-POSS (TPOSS) contains a partial T8 cage with one corner Si missing, leaving three Si–OH groups. It was used as-received (Scheme 2).

2.2. Preparation of PC/POSS hybrids

After polycarbonate was melted at 280 °C using a twin-roll mill (XK-160, Jiangsu, China), trisilanolphenyl-POSS (TPOSS) was added to the melted PC and blended for 10 min to yield the PC/TPOSS hybrids with different contents of TPOSS which were identified as PC/1 wt% TPOSS, PC/2 wt% TPOSS and PC/3 wt% TPOSS hybrids with the content of 1 wt%, 2 wt% and 3 wt% TPOSS, respectively. And the products were compressed into films in a 10 cm × 10 cm × 3 mm mold for 5 min at 290 °C.

2.3. Characterization

The samples for transmission electron microscopy (TEM) were cut from epoxy blocks with the embedded samples at

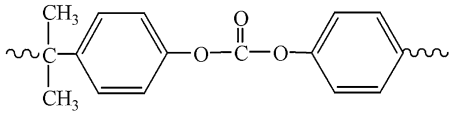

Scheme 1.

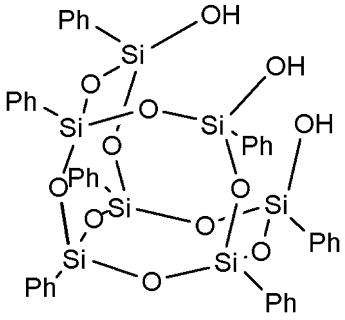

Scheme 2.

room temperature using an ultramicrotome (Ultracut-1, UK) with a diamond knife. Thin sections, 50–80 nm, were collected in a trough filled with water and then placed on 200-mesh copper grids. TEM images were obtained with a Hitachi H-800 microscope at an acceleration voltage of 100 kV. The thermogravimetric analyses (TGAs) and differential thermal analysis (DTA) of samples were carried out under air atmosphere with Netzsch STA409C thermal analyzer from 50 °C to 700 °C at a heating rate of 10 °C/min. The real time Fourier transform infrared spectra (FTIR) were recorded using a Nicolet MAGNA-IR 750 spectrophotometer equipped with a heating device and a temperature controller. Powders of samples were mixed with KBr powders, and the mixture was pressed into a tablet, which was then placed in a ventilated oven. The temperature of the oven was raised at a heating rate of 10 °C/min. The dynamic FTIR spectra were obtained in situ during the thermo-oxidative degradation processes. The cone calorimeter experiments were performed following the procedure defined in ISO 5660 on 3 mm thick 100 × 100 mm^2 plaques. Heat release rate and mass loss rate were obtained from the cone calorimetry experiments using online software. Typical results from cone calorimeter were reproducible within ±10% at a heat flux of 50 kW/m^2. Scanning electron microscopy (SEM) studies were performed on the surfaces and cross-sections of the char residues using a Hitachi X650 scanning electron microscope. The specimens were previously coated with a conductive layer of gold. X-ray photoelectron spectroscopy (XPS) was carried out with a VG Escalab Mark II spectrometer (VG Scientific Ltd, UK), using Al Kα excitation radiation ($h\nu = 1253.6$ eV).

3. Results and discussion

3.1. Morphology of PC/TPOSS hybrids

TEM observation was employed to characterize the size-scale level, the dispersion and morphology of TPOSS in the PC matrix. Fig. 1 shows the image for PC/3 wt% TPOSS hybrid with the content of 3 wt% TPOSS. The image clearly shows many blunt ellipsoidal TPOSS particles with a wide size distribution in the range of 20–300 nm. This suggests that the individual TPOSS molecules tend to aggregate together at a nanoscale level rather than becoming uniformly dispersed at a molecular level in the matrix. The formation

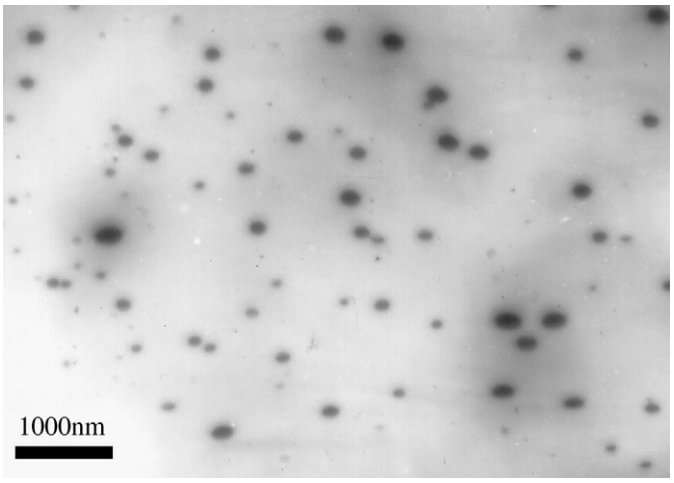

Fig. 1. TEM image of the PC/3 wt% TPOSS hybrid.

of TPOSS aggregates is probably dependent on many factors such as the melt crystallization of TPOSS [29], the incompatibility between the TPOSS and PC matrix and the formation of intermolecular hydrogen bonds of the hydroxyl groups between the TPOSS molecules. These all promote the aggregation of TPOSS.

Fig. 2 shows the FTIR spectra for bisphenol A polycarbonate (PC), trisilanolphenyl-POSS (TPOSS), and PC/3 wt% POSS hybrid. The structure of PC is shown in Scheme 1. The assignments of FTIR spectra of PC and TPOSS are listed in Table 1. The FTIR spectrum of the pristine PC possesses several characteristic absorption bands: the weak noise-like bands at 3400–3900 cm^{-1} and 1400–1900 cm^{-1} assigned to O–H stretching vibration of water; the CH_3 absorption bands at 2967 cm^{-1} and 2874 cm^{-1} corresponded to asymmetric and symmetric CH_3 stretching vibrations and the bands at 1465, 1386 and 1365 cm^{-1} corresponded to asymmetric and symmetric CH_3 deformation vibrations; the carbonate absorption bands at 1775 cm^{-1} assigned to the free carbonyl stretching vibration, the bands at 1235 cm^{-1}, 1194 cm^{-1}, 1163 cm^{-1} assigned to C–O stretching vibration; the *para*-substituted phenyl absorption bands including the bands at 3100–3000 cm^{-1} assigned to C–H stretching vibration of ring hydrogens, the weak bands at 2000–1660 cm^{-1} assigned to C–H deformation vibration of ring hydrogens, the bands at 1080 cm^{-1}, 1015 cm^{-1}, 831 cm^{-1} assigned to C–H deformation vibration of ring hydrogens, the bands at 1602 cm^{-1} and 1506 cm^{-1} assigned to C–C stretching vibration, the bands at 1386 cm^{-1} and 1365 cm^{-1} assigned to $C(CH_3)_2$ asymmetric bending vibration substituted phenyl, the weak band at 708 cm^{-1} assigned to ring deformation vibration.

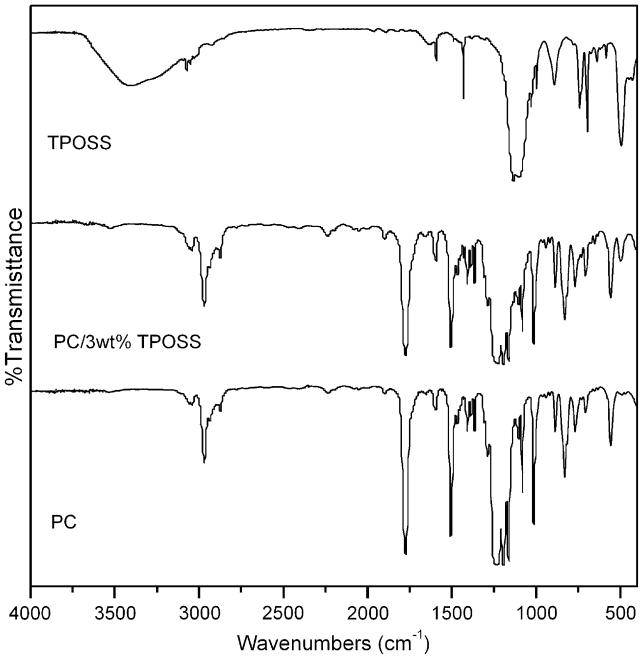

Fig. 2. FTIR spectra of PC, TPOSS and PC/3 wt% TPOSS.

Table 1
Assignment of FTIR spectra of PC and TPOSS

Wavenumber (cm^{-1})	Assignment
PC	
3400–3900, 1400–1900	O–H stretching vibration of water
2967, 2874	CH_3 stretching vibration
1465, 1386, 1365	CH_3 deformation vibration
1775	Free carbonyl stretching vibration
1235, 1194, 1163	C–O stretching vibration
3100–3000	C–H stretching vibration of phenyl ring hydrogens
2000–1660	C–H deformation vibration of phenyl ring hydrogens
1080, 1015, 831	C–H deformation vibration of phenyl ring hydrogens
1602, 1506	C–C stretching vibration of phenyl
1386, 1365	$C(CH_3)_2$ bending vibration of substituted phenyl
708	Phenyl ring deformation vibration
TPOSS	
3408	O–H stretching vibration of Si–O–H
893	Si–O stretching vibration
1134, 1103	Si–O–Si
430, 1028, 999	Si–phenyl stretching vibration
3100–3000	C–H stretching vibration of phenyl ring hydrogen
2000–1660	C–H deformation vibration of phenyl ring hydrogen
744	C–H deformation vibration of phenyl ring hydrogen
1630, 1594	C–C stretching vibration of phenyl
697	Phenyl ring deformation vibration

The structure of trisilanolphenyl-POSS (TPOSS) is shown in Scheme 2 and the FTIR spectrum of the pristine TPOSS shows several characteristic absorption bands: the Si–O–H absorption band including the broad strong band at 3408 cm^{-1} assigned to O–H stretching vibration (intermolecular hydrogen bands) and the band at 893 cm^{-1} assigned to Si–O stretching vibration; the bands at 1134 cm^{-1} and 1103 cm^{-1} assigned to Si–O–Si stretching vibration; the bands at 1430 cm^{-1}, 1028 cm^{-1}, 999 cm^{-1} assigned to Si–phenyl stretching vibration; the mono-substituted phenyl absorption band including the weak bands at 3100–3000 cm^{-1}

assigned to C–H stretching vibration of ring hydrogen, the weak bands at 2000–1660 cm^{-1} assigned to C–H deformation vibration of ring hydrogen, the band at 744 cm^{-1} assigned to C–H deformation vibration of ring hydrogen, the bands at 1630 cm^{-1} and 1594 cm^{-1} assigned to C–C stretching vibration, and the weak band at 697 cm^{-1} assigned to ring deformation vibration.

The FTIR spectrum of the PC/3 wt% TPOSS hybrid has the main absorption bands which appeared in pristine PC and TPOSS and does not have new apparent absorption bands. This indicates that there is no chemical reaction between TPOSS and PC during the melt blending process.

3.2. Thermal stability of PC/TPOSS hybrids

The TG, DTG and DTA curves of PC, TPOSS, PC/1 wt% TPOSS, PC/2 wt% TPOSS and PC/3 wt% TPOSS in Ar atmosphere are shown in Fig. 3(a)–(c). The onset degradation temperature of samples which was evaluated by the temperature of 10 wt% weight loss ($T_{-10\%}$), the mid-point temperature of the degradation ($T_{-50\%}$), the temperature of 70 wt% weight loss ($T_{-70\%}$) and the fraction of the solid residue that does not volatilize below 800 °C were obtained from the TG curve; the temperature of the maximum weight loss rate (T_{max}) of samples was obtained from the DTG curve; the temperature of the maximum exothermic peak (T_{mex}) of samples was obtained from the DTA curve. These data are listed in Table 2.

The thermal degradation process of the pristine TPOSS in Ar atmosphere has three stages in the temperature ranges of 20–120 °C, 120–300 °C and 300–800 °C corresponding to T_{max} of 43 °C, 210 °C and 568 °C, respectively. The solid residue at 800 °C is 56.1%. The weight losses of the first and second stages are only 3.3% and 4.1% that probably are derived from the elimination of the adsorption water of the TPOSS particles and the hydration water of the hydroxyl groups of TPOSS which can be verified by the weak endothermic peaks at 47 °C and 212 °C on DTA curve. A TPOSS molecule has three hydroxyl groups, but the hydroxyl groups cannot take exothermic condensation reaction between the TPOSS molecules. The reason probably is due to the steric effect of the T8 cage of TPOSS. The DTA curve of TPOSS shows broad endothermic peak and strong exothermic multi-peaks during the third stage including the complex reactions.

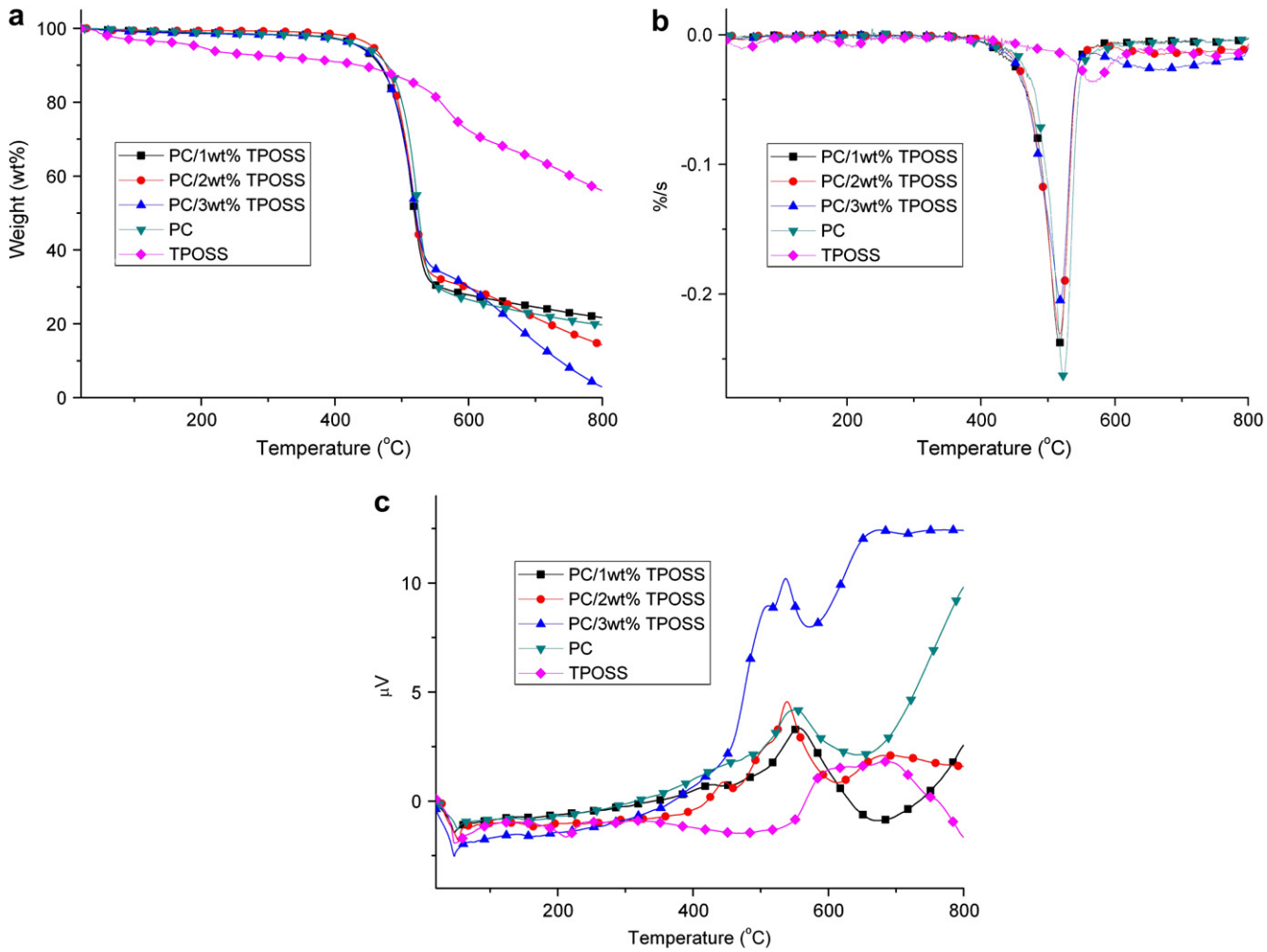

Fig. 3. (a) TG, (b) DTG and (c) DTA curves of PC, TPOSS, PC/1 wt% TPOSS, PC/2 wt% TPOSS and PC/3 wt% TPOSS in argon atmosphere.

Table 2
TG, DTG and DTA data in Ar of the samples

Samples	$T_{-10\%}$ (°C)	$T_{-50\%}$ (°C)	$T_{-70\%}$ (°C)	T_{max} (°C)	T_{mex} (°C)	Solid residue (%) at 800 °C
TPOSS	436	–	–	43, 210, 568	684	56.1
PC	478	525	553	524	552	19.7
PC/1 wt% TPOSS	467	508	557	517	558	21.7
PC/2 wt% TPOSS	477	514	596	518, 671	540	14.3
PC/3 wt% TPOSS	469	520	600	518, 670	538	2.9

This stage probably occurs the dissociation of the phenyl groups from TPOSS, the sublimation of TPOSS [30], the condensation of hydroxyl groups of the TPOSS molecules and the subsequent crosslinking reactions that incorporate the remaining composition into a polysiloxane network or char. Similar degradation process involving sublimation, condensation, partial loss of organic substituents followed by formation of SiO_xC_y networks has been observed for other kinds of POSS [31–33]. At last a ceramic residue is produced which is composed of silica containing a considerable amount of free carbon [30]. It is noted that the apparent reduction in char residue relative to that of ph-POSS is published by other studies [30]. The reason is probably due to the lower melting temperature relative to that of ph-POSS.

The thermal degradation process of PC in Ar atmosphere has only one stage corresponding to T_{max} of 524 °C. The DTA curve of PC shows that the sample presents continuous exothermic process with the increasing temperature. There is a strong exothermic peak at 552 °C on the DTA curve. Some complex chemical reactions are taken at the thermal degradation of PC which includes the chain scission of the isopropylidene linkage, hydrolysis/alcoholysis of carbonate linkage, reformation of carbonate linkage, and branching and crosslinking reaction of the molecular chains of PC [28]. Then the crosslinking polyaromatic carbonaceous residue is formed via crosslinking reactions at the higher temperature.

Fig. 3(a)–(c) shows the TG, DTG and DTA curves of the PC/1 wt% TPOSS, PC/2 wt% TPOSS and PC/3 wt% TPOSS in Ar atmosphere containing 1 wt%, 2 wt% and 3 wt% TPOSS, respectively. The thermal degradation process of PC/1 wt% TPOSS has one stage as the pristine PC. $T_{-10\%}$, $T_{-50\%}$ and T_{max} of PC/1 wt% TPOSS are all lower than those of PC. But T_{mex} and the fraction of the stable solid residue at 800 °C of PC/1 wt% TPOSS are slightly higher than those of PC. The thermal degradation process of the other PC/TPOSS samples becomes two stages with the TPOSS content increasing which is different from the pristine PC. $T_{-10\%}$, $T_{-50\%}$ and the fractions of the solid residue of PC/2 wt% TPOSS and PC/3 wt% TPOSS are all lower than those of PC. The two stages of thermal degradation process of the PC/TPOSS hybrids are in the temperature range of 20–560 °C and 560–800 °C corresponding to the T_{max} both around 518 °C and 670 °C. The exothermic peaks of both samples are multi-peaks, they are probably concealed by the strong peaks corresponding to T_{mex}. T_{mex} of both hybrids are lower than that of PC. Fig. 3(a)–(c) shows that TG/DTG/DTA curves in Ar atmosphere of PC/2 wt% TPOSS and PC/3 wt% TPOSS in the temperature range of 540–800 °C are all distinct from those of pristine PC. At about the temperature range of 540–620 °C, the weight loss of both hybrids is lower than that of PC. $T_{-70\%}$ of the hybrids at all levels is higher than that of PC due to the higher thermal stability of the intermediate products via the reactions between TPOSS and degradation products of PC macromolecule chains. PC can form more stable crosslinked polyaromatic carbonaceous residue [28], on the contrary, the intermediate products in PC/TPOSS decompose at higher temperature. So the fractions of the solid residue at 800 °C decrease with the content of increasing TPOSS.

Fig. 4(a)–(c) shows the TG, DTG and DTA curves of the pristine TPOSS, PC, PC/1 wt% TPOSS, PC/2 wt% TPOSS and PC/3 wt% TPOSS in air atmosphere. $T_{-10\%}$, $T_{-50\%}$, $T_{-70\%}$, T_{max}, T_{mex} and the fraction of the solid residue of all samples are listed in Table 3. Fig. 4(a)–(c) shows that the thermal oxidative degradation process of TPOSS has two stages in the temperature range of 50–400 °C and 400–800 °C corresponding to T_{max} of 207 °C and 645 °C and the stable solid residue at 800 °C is about 45.5 wt%. The first stage is only about 3 wt% derived from the elimination of the hydration water of the hydroxyl groups of TPOSS which can be verified by the weak endothermic peak at 210 °C on the DTA curve. The second stage corresponds to a strong exothermic peak at 628 °C on the DTA curve of TPOSS. During the second stage, with the increasing temperature, the phenyl groups dissociate from TPOSS, volatilize, and condense into crosslinking polysiloxane in the presence of oxygen. At high temperature, the polysiloxanes are further oxidized and decomposed to form the end product silicon dioxide and a few free carbons. This indicates that the volatilization, decomposition, condensation and oxidation reactions all take place at the second stage.

Fig. 4(a)–(c) also shows that the thermal oxidative degradation process of PC has two stages which is different from the thermal degradation process in Ar atmosphere of PC because of the presence of oxygen. The first stage is in the temperature range of 50–550 °C. Fig. 4(b) shows a strong peak at 508 °C corresponding to the first T_{max}, but there is a weaker shoulder peak at 477 °C before the peak. There are broad multiple exothermic peaks at 400–550 °C on the DTA curve of PC. These indicate that some complex chemical reactions take place at the first stage of thermal oxidative degradation including the free radical chain scission of the isopropylidene linkage and the branching and crosslinking reactions of molecular chains induced by oxygen besides the reactions in inert atmosphere. The second stage is in the temperature range of 550–800 °C corresponding to T_{max} of 609 °C, and the stable solid residue at 800 °C is about 3.7 wt%. A strong exothermic peak at 610 °C corresponds to the heat change of the second stage which is probably derived from the degradation and oxidation of the intermediate crosslinking products of PC. Lee [27] suggested that the initial step of the thermal oxidative degradation of PC is an oxidative hydrogen cleavage from the isopropylidene linkage and then

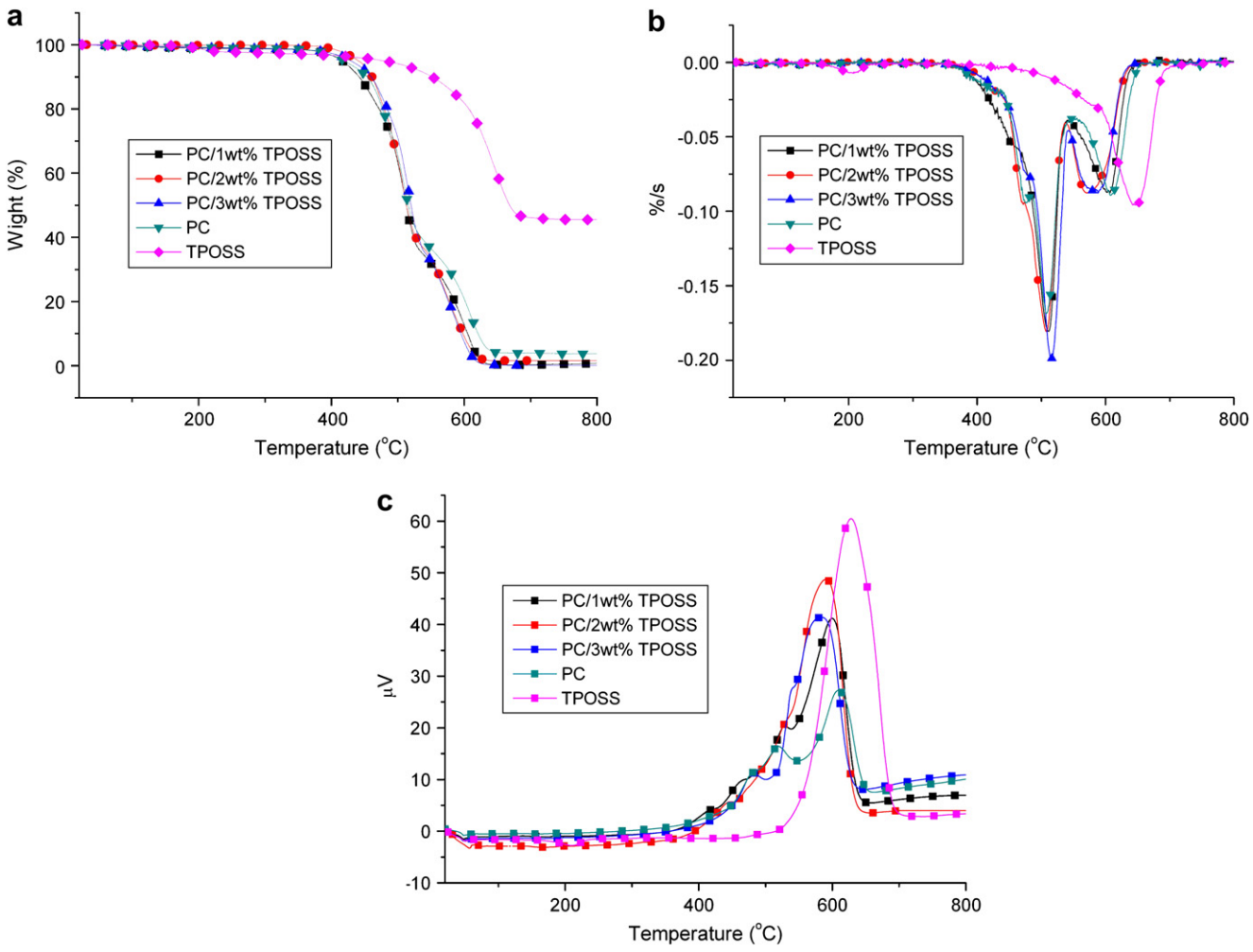

Fig. 4. (a) TG, (b) DTG and (c) DTA curves of PC, TPOSS, PC/1 wt% TPOSS, PC/2 wt% TPOSS and PC/3 wt% TPOSS in air atmosphere.

carbon–carbon bond scission, followed by hydrolysis and alcoholysis of the carbonate. Oxygen may facilitate free radical branching reaction via the formation of peroxides. And a highly crosslinked structure with diaryl ester, ether and unsaturated carbonaceous bridges is formed above 440 °C [28].

Fig. 4(a)–(c) shows the TG, DTG and DTA curves of the PC/1 wt% TPOSS, PC/2 wt% TPOSS and PC/3 wt% TPOSS in air, respectively. The thermal oxidative degradation process of all the hybrid samples has the similar two stages as the pristine PC. $T_{-10\%}$ of PC/1 wt% TPOSS is lower than that of PC. However, $T_{-10\%}$ of PC/TPOSS containing higher content of TPOSS (2 and 3 wt%) is higher than that of PC. $T_{-50\%}$ of PC/1 wt% TPOSS, PC/2 wt% TPOSS and PC/3 wt% TPOSS is close to that of PC, and it increases with the increase of TPOSS content. $T_{-70\%}$ and the fractions of the stable solid residue at 800 °C of PC/1 wt% TPOSS, PC/2 wt% TPOSS and PC/3 wt% TPOSS are all lower than those of PC. T_{mex} of PC/TPOSS is lower than that of PC, and the T_{mex} of PC/TPOSS decreases with the increasing TPOSS contents. These indicate that the incorporation of TPOSS can decrease the degradation stability of the PC/TPOSS hybrids in air.

Fig. 5(a) and (b) shows the dynamic FTIR spectra obtained from the thermal oxidative degradation of pure PC and PC/3 wt% TPOSS hybrids in the condensed phase at different temperatures, respectively, which can be used to study the beginning thermal oxidative degradation of the samples.

For pure PC, the main characteristic absorption bands are all present in the temperature range from room temperature to 300 °C, and the relative intensities and shapes of these characteristic absorption bands are primarily invariable. The intensities of these bands significantly decrease at 380 °C. The intensity of the weak noise-like bands at 3500–3900 cm^{-1} and 1400–1900 cm^{-1} assigned to water generation becomes stronger. The weak bands at about 3650 cm^{-1} assigned to the hydroxyl group derived from the alkyl substituted phenol producing from PC are observed. The

Table 3
TG, DTG and DTA data in air of the samples

Samples	$T_{-10\%}$ (°C)	$T_{-50\%}$ (°C)	$T_{-70\%}$ (°C)	$T_{\max}$ (°C)	T_{mex} (°C)	Solid residue (%) at 800 °C
TPOSS	552	668	–	207, 645	629	45.5
PC	454	516	576	508, 609	610	3.7
PC/1 wt% TPOSS	442	513	557	510, 607	600	0.7
PC/2 wt% TPOSS	461	513	559	510, 573	590	1.6
PC/3 wt% TPOSS	460	520	556	516, 584	584	0

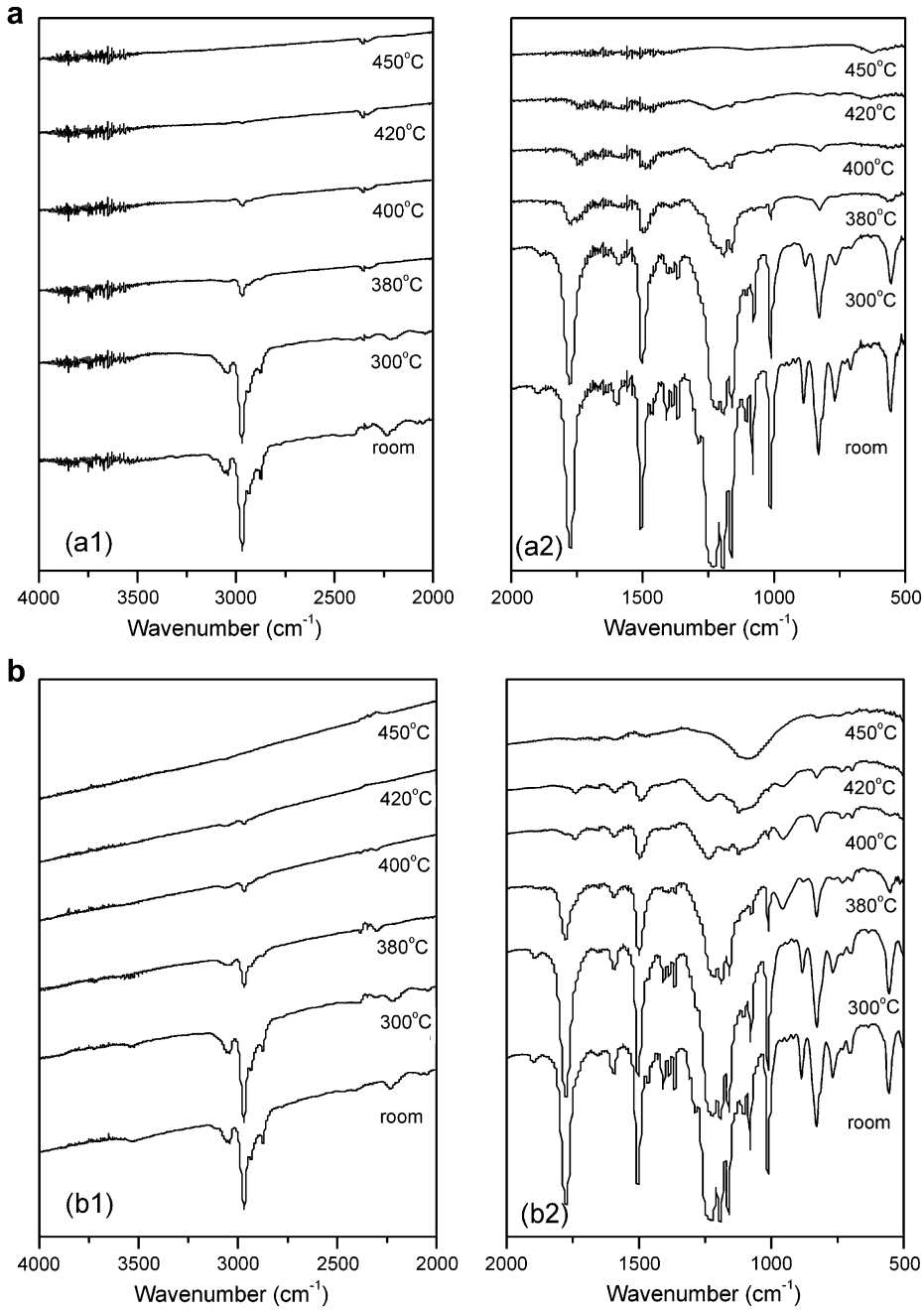

Fig. 5. The dynamic FTIR of (a) PC and (b) PC/3 wt% TPOSS.

peak of the carbonate characteristic absorption band at 1775 cm^{-1} becomes broad and form a new peak at the lower 1750 cm^{-1} range which may be attributed to the hydrogen bonding between the carbonate moiety and the phenols and several weak peaks around 1740–1640 cm^{-1} at 380 °C are observed which may be the products of the hydrolysis/alcoholysis and thermo-oxidation with different carbonyl functional groups including the ester, aldehyde, carboxylic acid and ketone groups [28]. This indicates that the PC matrix has already taken some thermo-oxidative reactions at this temperature. The intensities of the intrinsic bands further decrease so that some relative weaker bands disappear with the temperature further increasing to 400 °C. The absorption band of carbonyl group at 1775 cm^{-1} shifts to 1745 cm^{-1}. These absorption bands are weakened significantly at 450 °C, and the weak bands at around 3900–3500 cm^{-1}, 1600–1300 cm^{-1}, 1200–1000 cm^{-1}, 625 cm^{-1} may be corresponding to polyaromatic substituted phenols [34]. The TG curve shows that PC only losses about 10 wt% at 450 °C. It is concluded that some branched and crosslinked structures with various carbonyl groups, ether and unsaturated carbonaceous bridges are produced at the beginning of the thermal oxidative degradation.

The dynamic FTIR spectra of PC/1 wt% TPOSS and PC/2 wt% TPOSS are almost coincident with those of PC/3 wt%

TPOSS except for the relative intensity between the hybrids, so only the spectrum of PC/3 wt% TPOSS is provided. The FTIR spectrum of the hybrid at 380 °C has some differences from that of the hybrid at room temperature. A new absorption band at about 956 cm^{-1} assigned to Si–O–phenyl stretching vibration is observed. At the same time, the weak and noise-like bands at 3500–3900 cm^{-1} and 1300–1900 cm^{-1} assigned to water and the alkyl substituted phenols are observed; and the peak of the carbonate characteristic absorption band at 1775 cm^{-1} widens but does not shift and the bands around 1830–1660 cm^{-1} also does not appear. These confirm that the Si–O–H groups of TPOSS preferably react with the aliphatic substituted phenol to obtain Si–O–phenyl group. The band at about 1430 cm^{-1} assigned to Si–phenyl group is weakened which means that the phenyl group is dissociated from TPOSS. The formation of phenyl and silicon radicals derived from the dissociation of TPOSS would retard the free radical oxidative reactions of the PC matrix through eliminating the high reactive hydrogen and hydroxy radicals. Therefore the thermal oxidative stability of the PC matrix is increased. While the temperature increases to 400 °C, a new peak at 1745 cm^{-1} forms and the weak peaks at around 1830–1660 cm^{-1} appear as those of the pristine PC at 380 °C. And with the relative intensity of the bands of C–O–C group at 1230–1150 cm^{-1} decreasing, that of the bands of Si–O–Si group at 1130–1000 cm^{-1} increase. With the increasing temperature, the relative intensity of the bands of Si–O–phenyl group at 956 cm^{-1} decreases and the relative intensity of the broad bands of Si–O–Si group at 1130–1000 cm^{-1} increases. At 450 °C, only a broad peak at 1100 cm^{-1} assigned to Si–O–Si group remains and the bands assigned to Si–ph and Si–O–ph groups disappear. It is likely that the Si–Oph and Si–ph bonds both transfer into Si–O–Si bonds which mean the formation of polysiloxane derivatives. And with the temperature further increasing, polysiloxane derivatives finally may be oxidized and degraded to form silicon dioxide.

At the beginning stage of thermal degradation of PC in inert atmosphere, the reactions between TPOSS and the alkyl substituted phenols derived from the hydrolysis/alcoholysis products of PC [25] are taken to form the branching intermediate products containing –Si–O–phenyl group (Scheme 3) because of the high reactivity of the Si–OH of TPOSS which can enhance the thermal stability of matrix with the increasing temperature. But the reaction between TPOSS and the alkyl substituted phenols can release water which also participates in the hydrolysis reaction of PC. The accelerated hydrolysis/alcoholysis of PC can eliminate more carbonate groups which would probably impair the reformation of the carbonate group (Scheme 4) [25] and the consequential branching reaction of PC which is the precondition of the formation of the crosslinking polyaromatic carbonaceous residue at higher temperature. The intermediate products containing –Si–O–phenyl group embed in the impaired structure of crosslinking polyaromatic chains. At the higher temperature, the SiO–phenyl bonds of the intermediate products containing –Si–O–phenyl group are cleaved, and crosslinking reaction takes place between TPOSS molecules to form crosslinking polysiloxane. The

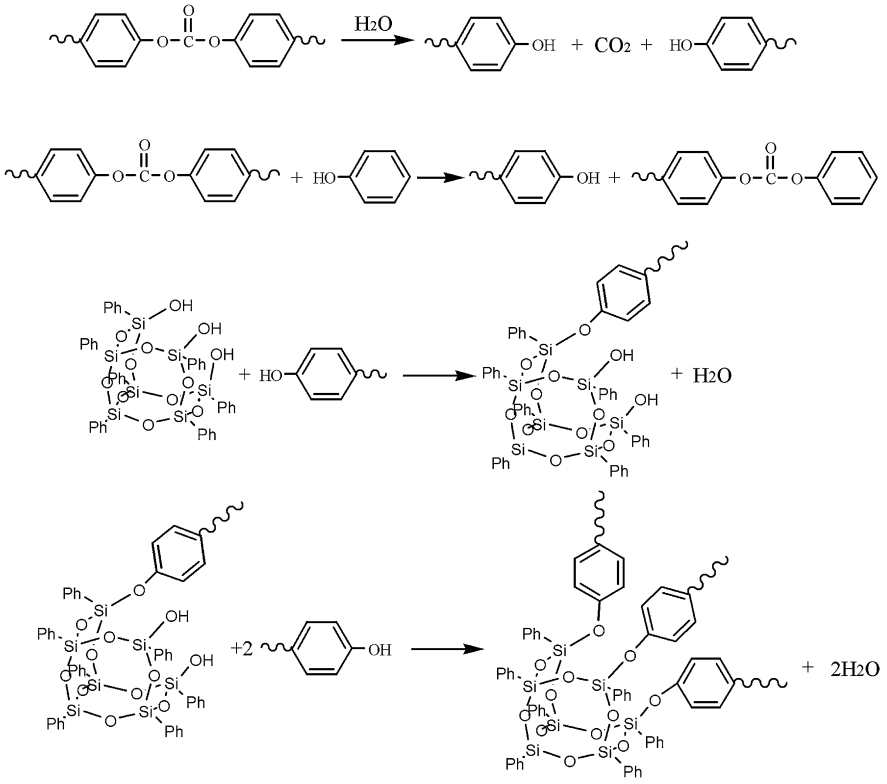

Scheme 3.

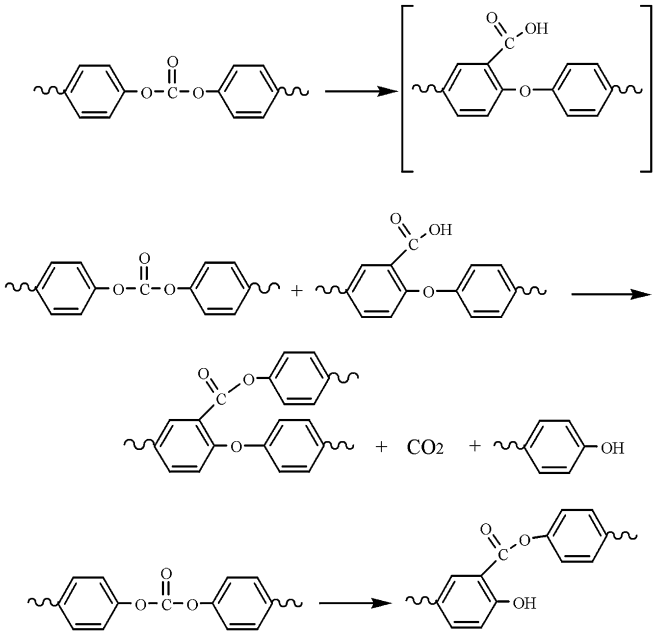

Scheme 4.

structure of crosslinked polyaromatic carbonaceous residue is impaired so that the thermal stability of the carbonaceous residue is further decreased. These also explain the lower thermal stability observed when comparing to pristine PC.

The thermal oxidative degradation of PC in air takes all the reactions as those of the thermal degradation in inert atmosphere. Moreover, the presence of oxygen can induce the chain scission of the isopropylidene linkage via free radical oxidative degradation and the branching reactions (Scheme 5) [28]. At the beginning stage of thermal oxidative degradation, the onset thermal degradation temperature of PC is decreased because of the free radical oxidative degradation compared with that in inert atmosphere. With the increasing temperature, the inducement of oxygen accelerates the formation of the crosslinked polyaromatic carbonaceous residue. TPOSS can interfere with the free radical oxidative degradation process of PC. The phenyl radical can dissociate from TPOSS at lower temperature in the presence of water and the acidic condition, and the silicon radical is formed. The phenyl radical can capture the hydrogen radical and the silicon radical can capture the hydroxy radical. TPOSS can play a role of radical trap via consuming the high reactive hydrogen and hydroxy radicals so that they increase the onset degradation temperature of the matrix. And TPOSS can react with the alkyl substituted phenols to form the branched and crosslinked intermediate siloxane products which results in the enhancement of the thermal oxidative stability of PC matrix at lower temperature. However, TPOSS also can trap the aryl and alkyl radicals which interfere the formation of crosslinked polyaromatic carbonaceous residue at higher temperature. And the formed intermediate siloxane products impair the formation of crosslinked polyaromatic carbonaceous residue. The thermal oxidative stability of these intermediate siloxane products is lower than that of the polyaromatic carbonaceous residue at higher temperature. With the increasing temperature, they are decomposed so that the thermal oxidative stability of the carbonaceous residue is further decreased. In addition, the effects of TPOSS on thermal stability of PC result from not only the chemical reactions between TPOSS and degradation products of the PC matrix but also from the volatilization of TPOSS [30].

3.3. Flame retardant properties of PC/TPOSS hybrids

The heat release rate (HRR) was measured by cone calorimeter; HRR peak (PHRR) has been considered to be the most important parameter to evaluate the fire safety of polymeric materials. Fig. 6 shows that the pure PC is burnt slowly after ignition under a heat flux of 50 kW/m^2. PC is charred rapidly during the combustion. Methane in the volatile products of PC is the highly volatile and highly combustible gas which is most likely important for PC ignition [25]. Table 4 lists the cone data of all the samples. Table 3 shows that the ignition time (t_{ign}) of pure PC is 72 s. The addition of TPOSS results t_{ign} forward. Table 3 shows that t_{ign} of PC/1 wt% TPOSS, PC/2 wt% TPOSS and PC/3 wt% TPOSS are 54 s, 52 s, 41 s, respectively, which are all less than those of pure PC and decrease with the increasing content of TPOSS. Fig. 6 shows that the combustion process of pure PC presents a sharp peak on the HRR curve and the PHRR is 492 kW/m^2. The combustion process of PC/1 wt% TPOSS and PC/2 wt% TPOSS presents multi-peaks on the HRR curve. The presence of TPOSS decreases the maximum PHRR compared with that of the pure PC; the value of maximum PHRR decreases with the increasing content of TPOSS; the time to the maximum PHRR (t_p) decreases with the increasing content of TPOSS. The maximum PHRR of PC/2 wt% TPOSS with 2 wt% content of TPOSS is 267 kW/m^2 which is 45.7% lower than PHRR of the pure PC. There is a smaller peak after the maximum peak on the HRR curve of the above two hybrid samples which are different from the pure PC. This shows that the presence of TPOSS possibly affects the combustion process of the PC matrix, and the smaller peak decreases with the increasing content of TPOSS. With regard to PC/3 wt% TPOSS, its combustion process is different for the above two hybrids. When the loading amount of TPOSS is increased from 2 wt% to 3 wt%, the PHRR increases to 320 kW/m^2; its combustion process presents only one peak and the smaller peak disappears on the HRR curve. Another primary parameter which is relevant to HRR is the mass loss rate (MLR) during combustion. Table 3 lists the maximum value of MLR of the samples. This indicates that the trend of the evolution of the MLR is the same as the change of the maximum value of HRR of the samples, and the peaks of CO concentration (PCOC) (Fig. 6(b)) in the combustion are also obviously decreased. The trend of the evolution of the PCOC is also same as that of the HRR of the samples. But after 300 s, the COC curves all appear as a broad peak corresponding to the char combustion. These indicate that the addition of TPOSS does affect the combustion behaviors of the PC matrix and increase the flame retardant

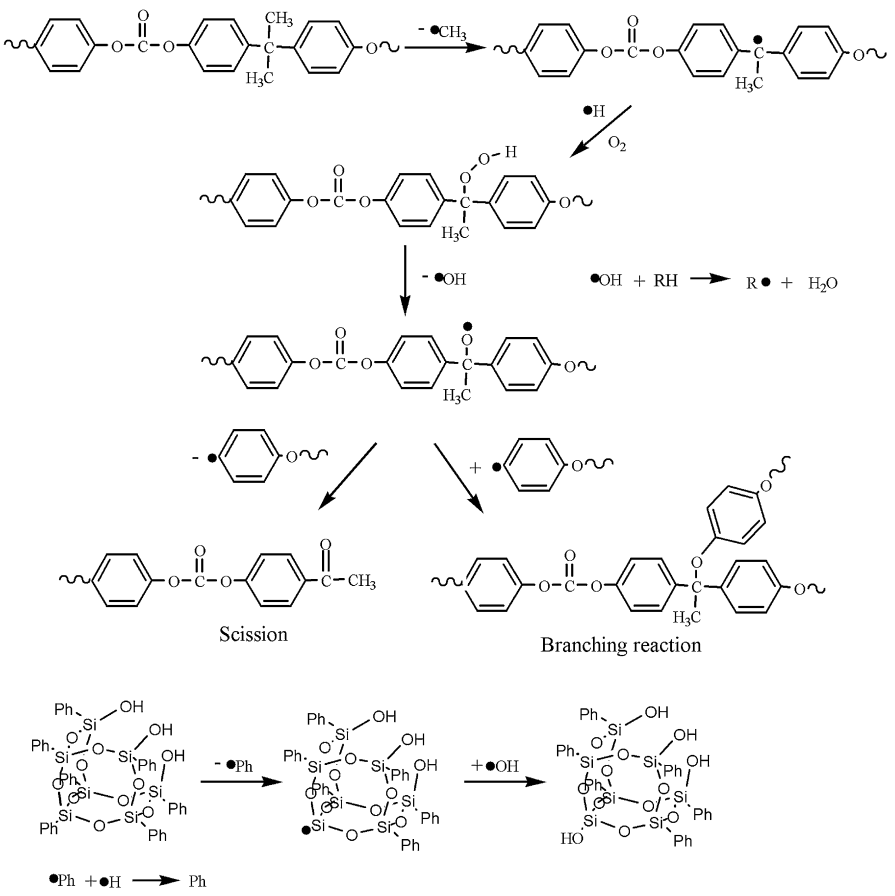

Scheme 5.

properties of the matrix. The similar flame retardant properties of POSS were reported by other publications [35,36].

3.4. SEM and XPS analyses

Fig. 7 shows the SEM photographs obtained for the exterior and interior char residues of the pure PC and PC/2 wt% TPOSS samples. The exterior char residue of the pure PC presents a porous surface with micro-size pores. The interior char residue of the pure PC presents a smooth and continual char layer which means the rapid volatilization at the surface. The exterior char residue of PC/2 wt% TPOSS presents some holes and many closed and leakage bubbles. Its interior char residue mainly presents a smooth and continual char layer on which are dispersed some bubbles and folds. This means that the incorporation of TPOSS restricts the rapid

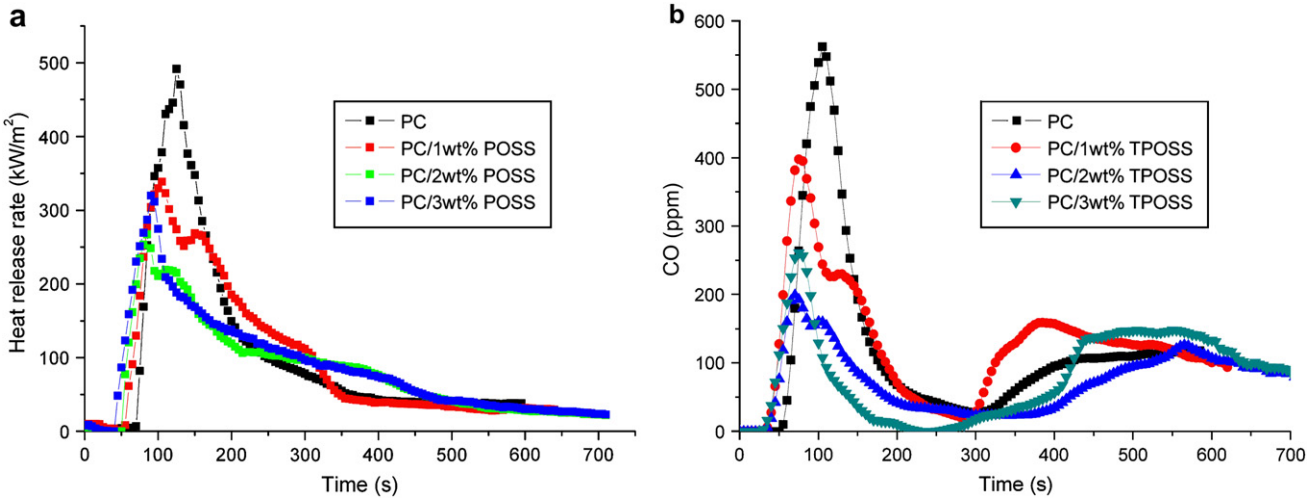

Fig. 6. (a) HRR and (b) COC plots of the PC, PC/1 wt% TPOSS, PC/2 wt% TPOSS and PC/3 wt% TPOSS.

Table 4
Some cone data of the samples

	t_{ign} (s)	PHRR (kW/m^2)	MLR (g/m^2 s)	PCOC (ppm)
PC	72	492	0.236	562.3
PC/1 wt% TPOSS	54	339	0.178	397.9
PC/2 wt% TPOSS	52	267	0.148	199.3
PC/3 wt% TPOSS	41	320	0.173	261.2

volatilization at the surface and enhances the flame resistance of the exterior char residue.

The exterior and interior char residues of the pure PC and PC/2 wt% TPOSS are investigated by XPS analysis. The C1s, O1s and Si2p spectra of samples are shown in Table 5 which summarizes the results of the most probable fit assumption. For C1s spectrum of the pure PC has four peaks [37]: the peak at around 284.7 eV is attributed to C–H and C–C in aromatic species, the peak at around 286.3 eV is assigned to C–O (ether and/or hydroxyl group), and the other peaks corresponded to carbonyl (at around 287.7 eV) and carboxyl (at around 289 eV) groups. For O1s spectrum, PC has two peaks at around 531.5 and 533.6 eV which can be assigned to =O in carbonyl groups and –O– in C–O groups, respectively.

For the pristine PC, the atom percent of oxygen in the exterior char residue is higher than that in the interior char residue. And the atom percent of carbon in aromatic species in the exterior char residue is lower than that in the interior char residue. The reason is that the exterior char residue is highly oxidized under the rich oxygen condition. Additionally, PC has a weak peak on Si2p at around 102.6 eV assigned to Si–O in the exterior char residue. The atom percent of Si is only 0.25% which probably is derived from the processing agent.

For the PC/2 wt% TPOSS hybrid, the atom percents of carbon, oxygen and silicon in exterior and interior char residues are all listed in Table 2. The atom percent of Si in exterior and interior char residues is 5.02% and 0.54%, respectively, namely, the content of SiO_2 in exterior char residue is much higher than that in the interior char residue. This result implies that SiO_2 can be accumulated or pushed by the bubbles on the surface of burning PC. The ratios between unoxidized carbon and oxidized carbon of PC/2 wt% TPOSS are higher than those of PC in exterior and interior char residues. It is indicated that the incorporation of TPOSS retards the oxidation of char residue.

During the combustion process, the thermal oxidative degradation of PC matrix proceeds very quickly and violently under a high temperature. This process cannot be explained by the above thermal oxidative degradation mechanism. The effect of TPOSS on combustion behaviors could be summarized: under the high temperature, a char layer is formed on the surface of the matrix; a fast degradation is preceded in the matrix. TPOSS quickly undergoes a series of oxidation reactions to form SiO_2 in the matrix and releases more combustible small molecules such as benzene dissociated from TPOSS, so the time to ignition of hybrids decreases. Quite a few SiO_2 is pushed on the surface of the matrix by the volatile products such as phenol derivates, methane, CO, CO_2. And the presence of SiO_2 can enhance the viscosity

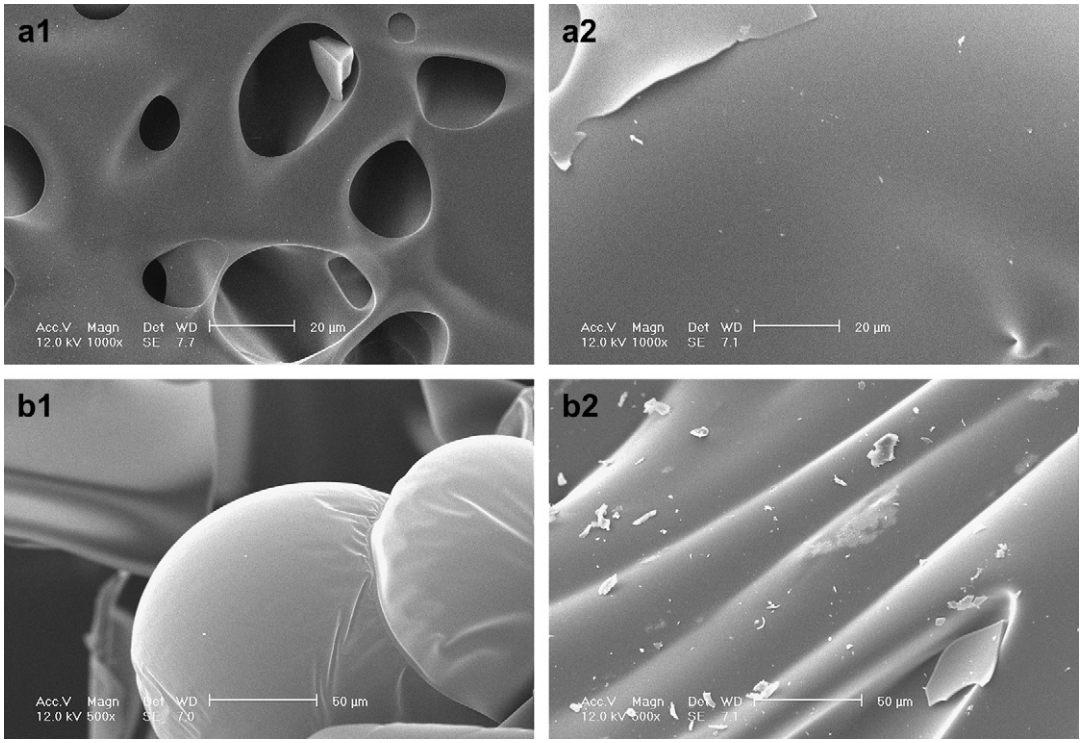

Fig. 7. SEM images of the (1) exterior and (2) interior char residues of (a) PC and (b) PC/2 wt% TPOSS.

Table 5
XPS data of the samples

PC	Binding energy (eV)	Area (%)	PC/2 wt% TPOSS	Binding energy (eV)	Area (%)
Exterior char residue					
C1s (C–H, C–C)	284.74	56.36	C1s (C–H, C–C)	284.71	48.74
C1s (C–O)	286.29	17.13	C1s (C–O)	286.29	9.35
C1s (C=O)	287.74	4.85	C1s (C=O)	287.63	2.83
C1s (–COOH)	289	4.17	C1s (–COOH)	289	3.36
O1s (=O)	531.53	7.17	O1s (=O)	531.2	2.17
O1s (–O–)	533.61	10.06	O1s (–O–)	533.5	28.52
Si2p	102.61	0.25	Si2p	103.55	5.02
Interior char residue					
C1s (C–H, C–C)	284.65	80.45	C1s (C–H, C–C)	284.70	79.23
C1s (C–O)	286.28	6.1	C1s (C–O)	286.70	4.44
C1s (C=O)	287.52	2.29	C1s (C=O)	287.74	0.48
C1s (–COOH)	289	2.49	C1s (–COOH)	289.03	3.48
O1s (=O)	531.53	4.98	O1s (=O)	531.2	6.05
O1s (–O–)	533.61	3.68	O1s (–O–)	533.7	5.79
Si2p	0	0	Si2p	103.55	0.54

and thermal oxidative stability of the char layer which builds up on the surface of the burning polymer, insulates the heat transformation and the dispersion of oxygen into underlying polymeric substrate to prevent thermo-oxidative reactions, and prevents the release of volatile products of underlying polymeric substrate from the matrix. So the value of HRR of hybrids decreases. The competitive effects of TPOSS on the improvement of the amount of combustible small molecules at the early stage of the combustion and enhancement of viscosity and stability of the char layer result in a balance for flame retardant effect of TPOSS.

4. Conclusion

The polycarbonate/polyhedral oligomeric silsesquioxane hybrids were prepared based on bisphenol A polycarbonate (PC) and trisilanolphenyl-POSS (TPOSS) by the melt blending method. The determination of transmission electronic microscopy (TEM) and Fourier transform infrared spectroscopy (FTIR) confirmed that the elliptical nanoscale TPOSS particles disperse in the PC matrix. Moreover, TPOSS did not react with the PC matrix during the melt blending process. The thermal stability of the PC/TPOSS hybrids in argon and air was investigated. The thermal oxidative degradation process of PC/TPOSS hybrid is very complicated which include the chemical reactions of the hydrolysis/alcoholysis of carbonate linkage, chain scission of the isopropylidene linkage, the free radical oxidative chain degradation, the reformation, the branching and crosslinking reactions. At the beginning of the thermal degradation of PC matrix, TPOSS can react with the alkyl and aromatic substituted phenols and the high reactive free radicals derived from the thermal oxidative degradation of PC which simultaneously interfere with the decomposing and crosslinking processes of PC matrix at lower temperature. With the increasing temperature, the presence of TPOSS induces the formation of volatile degradation products and reduces the char formation of the PC matrix. The flame retardant properties of the hybrids were evaluated by cone calorimetry experiments. The addition of TPOSS significantly decreased the peak heat release rate (PHRR) of the hybrids, although the presence of POSS shortened the ignition time at all levels tested. Scanning electronic microscopy (SEM) and X-ray photoelectron spectroscopy (XPS) were used to explore the char residues of the pure PC and the hybrids. The incorporation of TPOSS retards the oxidation of char residue and enhances the intensity and thermal oxidative stability of the char layer which builds up on the surface of the burning polymer.

Acknowledgment

The work was financially supported by the National Natural Science Foundation of China (No. 50403014).

References

[1] Laine RM. Nanobuilding blocks based on the $[OSiO_{1.5}]_x$ ($x = 6$, 8, 10) octasilsesquioxanes. J Mater Chem 2005;15(35–36):3725–44.
[2] Baney RH, Itoh M, Sakakibara A, Suzuki T. Silsesquioxanes. Chem Rev 1995;95(5):1409–30.
[3] Li GZ, Wang LC, Ni HL, Pittman CU. Polyhedral oligomeric silsesquioxane (POSS) polymers and copolymers: a review. J Inorg Organomet Polym 2001;11(3):123–54.
[4] Liu L, Hu Y, Song L, Nazare S, He SQ, Hull R. Combustion and thermal properties of octaTMA-POSS/PS composites. J Mater Sci 2007;42(12):4325–33.
[5] Fu BX, Yang L, Somani RH, Zong SX, Hsiao BS, Phillips S, et al. Crystallization studies of isotactic polypropylene containing nanostructured polyhedral oligomeric silsesquioxane molecules under quiescent and shear conditions. J Polym Sci Polym Phys 2001;39(22):2727–39.
[6] Fina A, Tabuani D, Frache A, Camino G. Polypropylene–polyhedral oligomeric silsesquioxanes (POSS) nanocomposites. Polymer 2005;46(19):7855–66.
[7] Liu L, Tian M, Zhang W, Zhang LQ, Mark JE. Crystallization and morphology study of polyhedral oligomeric silsesquioxane (POSS)/polysiloxane elastomer composites prepared by melt blending. Polymer 2007;48(11):3201–12.

[8] Baldi F, Bignotti F, Fina A, Tabuani D, Ricco T. Mechanical characterization of polyhedral oligomeric silsesquioxane/polypropylene blends. J Appl Polym Sci 2007;105(2):935–43.
[9] Madbouly SA, Otaigbe JU, Nanda AK, Wicks DA. Rheological behavior of POSS/polyurethane–urea nanocomposite films prepared by homogeneous solution polymerization in aqueous dispersions. Macromolecules 2007;40(14):4982–91.
[10] Zhang ZP, Liang GZ, Wang JL, Ren PG. Epoxy/POSS organic–inorganic hybrids: viscoelastic, mechanical properties and micromorphologies. Polym Compos 2007;28(2):175–9.
[11] Xiao F, Sun YY, Xiu YH, Wong CP. Preparation, thermal and mechanical properties of POSS epoxy hybrid composites. J Appl Polym Sci 2007; 104(4):2113–21.
[12] Wu J, Haddad TS, Kim GM, Mather PT. Rheological behavior of entangled polystyrene–polyhedral oligosilsesquioxane (POSS) copolymers. Macromolecules 2007;40(3):544–54.
[13] Kopesky ET, McKinley GH, Cohen RE, Lichtenhan JD, Gilman JW, Ismail IMK. Toughened poly(methyl methacrylate) nanocomposites by incorporating polyhedral oligomeric silsesquioxanes. Polymer 2006; 47(1):299–309.
[14] Baldi F, Bignotti F, Ricco L, Monticelli O, Ricco T. Mechanical and structural characterization of POSS-modified polyamide 6. J Appl Polym Sci 2006;100(4):3409–14.
[15] Joshi M, Butola BS, Simon G, Kukaleva N. Rheological and viscoelastic behavior of HDPE/octamethyl-POSS nanocomposites. Macromolecules 2006;39(5):1839–49.
[16] Zhang WH, Fu BX, Seo Y, Schrag E, Hsiao B, Mather PT, et al. Effect of methyl methacrylate/polyhedral oligomeric silsesquioxane random copolymers in compatibilization of polystyrene and poly(methyl methacrylate) blends. Macromolecules 2002;35(21):8029–38.
[17] Fu BX, Hsiao BS, Pagola S, Stephens P, White H, Rafailovich M, et al. Structural development during deformation of polyurethane containing polyhedral oligomeric silsesquioxanes (POSS) molecules. Polymer 2001;42(2):599–611.
[18] Hsiao BS, White H, Rafailovich M, Mather PT, Jeon HG, Phillips S, et al. Nanoscale reinforcement of polyhedral oligomeric silsesquioxane (POSS) in polyurethane elastomer. Polym Int 2000;49(5):437–40.
[19] Mather PT, Jeon HG, Romo-Uribe A, Haddad TS, Lichtenhan JD. Mechanical relaxation and microstructure of poly(norbornyl-POSS) copolymers. Macromolecules 1999;32(4):1194–203.
[20] Romo-Uribe A, Mather PT, Haddad TS, Lichtenhan JD. Viscoelastic and morphological behavior of hybrid styryl-based polyhedral oligomeric silsesquioxane (POSS) copolymers. J Polym Sci Polym Phys 1998; 36(11):1857–72.
[21] Kim GM, Qin H, Fang X, Sun FC, Mather PT. Hybrid epoxy-based thermosets based on polyhedral oligosilsesquioxane: cure behavior and toughening mechanisms. J Polym Sci Polym Phys 2003;41(24): 3299–313.
[22] Lee A, Lichtenhan JD. Thermal and viscoelastic property of epoxy-clay and hybrid inorganic–organic epoxy nanocomposites. J Appl Polym Sci 1999;73(10):1993–2001.
[23] Zhao YQ, Schiraldi DA. Thermal and mechanical properties of polyhedral oligomeric silsesquioxane (POSS)/polycarbonate composites. Polymer 2005;46(25):11640–7.
[24] Pham HT, Munjal S, Bosnyak CP. Polycarbonates. In: Olabisi O, editor. Handbook of thermoplastics. New York: Marcel Dekker; 1997.
[25] Levchik SV, Weil ED. Overview of recent developments in the flame retardancy of polycarbonates. Polym Int 2005;54(7):981–98.
[26] Davis A. Stability of polycarbonate. J Macromol Sci Rev Macromol Chem Phys 1969;3:49.
[27] Lee LH. Mechanisms of thermal degradation of phenolic condensation polymers. I. Studies on thermal stability of polycarbonate. J Polym Sci A – Gen Pap 1964;2:2859.
[28] Jang BN, Wilkie CA. The thermal degradation of bisphenol A polycarbonate in air. Thermochim Acta 2005;426(1–2):73–84.
[29] Waddon AJ, Zheng L, Farris RJ, Coughlin EB. Nanostructured polyethylene–POSS copolymers: control of crystallization and aggregation. Nano Lett 2002;2(10):1149–55.
[30] Fina A, Tabuani D, Carniato F, Frache A, Boccaleri E, Camino G. Polyhedral oligomeric silsesquioxanes (POSS) thermal degradation. Thermochim Acta 2006;440(1):36–42.
[31] Mantz RA, Jones PF, Chaffee KP, Lichtenhan JD, Gilman JW, Ismail IMK, et al. Thermolysis of polyhedral oligomeric silsesquioxane (POSS) macromers and POSS–siloxane copolymers. Chem Mater 1996;8(6):1250–9.
[32] Liu YR, Huang YD, Liu L. Effects of TriSilanolIsobutyl–POSS on thermal stability of methylsilicone resin. Polym Degrad Stab 2006;91(11): 2731–8.
[33] Liu YR, Huang YD, Liu L. Thermal stability of POSS/methylsilicone nanocomposites. Compos Sci Technol 2007;67(13):2864–76.
[34] Huang XB, Ouyang XY, Ning FL, Wang JQ. Mechanistic study on flame retardance of polycarbonate with a small amount of potassium perfluorobutane sulfonate by TGA–FTIR/XPS. Polym Degrad Stab 2006;91(3): 606–13.
[35] Devaux E, Rochery M, Bourbigot S. Polyurethane/clay and polyurethane/POSS nanocomposites as flame retarded coating for polyester and cotton fabrics. Fire Mater 2002;26(4–5):149–54.
[36] Jash P, Wilkie CA. Effects of surfactants on the thermal and fire properties of poly(methyl methacrylate)/clay nanocomposites. Polym Degrad Stab 2005;88(3):401–6.
[37] Zhu SW, Shi WF. Thermal degradation of a new flame retardant phosphate methacrylate polymer. Polym Degrad Stab 2003;80(2):217–22.